

1 **2. Supplementary Information:**2 **A. Flat Files**

3

Item	Present?	Filename This should be the name the file is saved as when it is uploaded to our system, and should include the file extension. The extension must be .pdf	A brief, numerical description of file contents. i.e.: <i>Supplementary Figures 1-4, Supplementary Discussion, and Supplementary Tables 1-4.</i>
Supplementary Information	Yes	LIG_MOT_supplement.pdf	Supplementary Figures 1-8, Supplementary Discussion, and Supplementary Tables 1-4.
Reporting Summary	No		

4

5

6

7

8

9

10

Global ocean heat content in the Last Interglacial

11 Shackleton, S.^{1*}, Baggenstos, D.², Menking, J.A.³, Dyonisius, M.N.⁴, Bereiter, B.^{2,5}, Bauska,
 12 T.K.⁶, Rhodes, R.H.⁷, Brook, E.J.³, Petrenko, V.V.⁴, McConnell, J.R.⁸, Kellerhals, T.², Häberli,
 13 M.², Schmitt, J.², Fischer, H.², Severinghaus, J.P.¹

14 ¹Scripps Institution of Oceanography, University of California, San Diego, La Jolla CA, USA

15

16 ²Climate and Environmental Physics, Physics Institute and Oeschger Center for Climate Change
 17 Research, University of Bern, Bern, Switzerland

18

19 ³ College of Earth, Ocean, and Atmospheric Sciences, Oregon State University, Corvallis OR,
 20 USA

21

22 ⁴ Earth & Environmental Sciences, University of Rochester, Rochester NY, USA

23

24 ⁵ Laboratory for Air Pollution / Environmental Technology, Empa, 8600 Dübendorf, Switzerland

25

26 ⁶ British Antarctic Survey, Cambridge, UK

27

28 ⁷ Department of Earth Sciences, University of Cambridge, Cambridge, UK

29

30 ⁸ Division of Hydrologic Sciences, Desert Research Institute, Reno NV, USA

31

32 *Corresponding author: Sarah Shackleton, sshackle@ucsd.edu

33

34 **Abstract**

35 The Last Interglacial (129-116 ka) represents one of the warmest climate intervals of the last
36 800,000 years and the most recent time when sea level was meters higher than today. However, the
37 timing and magnitude of peak warmth varies between reconstructions, and the relative importance of
38 individual sources contributing to elevated sea level (mass gain versus seawater expansion) during the
39 Last Interglacial remains uncertain. Here we present the first mean ocean temperature record for this
40 interval from noble gas measurements in ice cores and constrain the thermal expansion contribution
41 to sea level. Mean ocean temperature reaches its maximum value of $1.1\pm 0.3^{\circ}\text{C}$ warmer-than-modern
42 at the end of the penultimate deglaciation at 129 ka, resulting in $0.7\pm 0.3\text{m}$ of elevated sea level,
43 relative to present. However, this maximum in ocean heat content is a transient feature; mean ocean
44 temperature decreases in the first several thousand years of the interglacial and achieves a stable,
45 comparable-to-modern value by ~ 127 ka. The synchronicity of the peak in mean ocean temperature
46 with proxy records of abrupt transitions in oceanic and atmospheric circulation suggests that the mean
47 ocean temperature maximum is related to the accumulation of heat in the ocean interior during the
48 preceding period of reduced overturning circulation.

49

50

51 **Introduction**

52 With a heat capacity one thousand times larger than that of the atmosphere, the ocean plays
53 an important role in regulating the rate and magnitude of global temperature change and represents
54 the largest energy reservoir in the climate system¹. Ocean heat uptake and warming contribute
55 directly to increasing sea level through thermal expansion of seawater and may play a role in future
56 sea level rise through enhanced sub-shelf melting and subsequent mass loss from the Antarctic Ice
57 Sheet². To understand the future role of ocean heat uptake, it is instructive to study ocean temperature
58 change during past warm periods in Earth's history.

59 During the Last Interglacial (LIG, 129-116 ka) surface temperatures were warmer than today,
60 but existing reconstructions differ substantially on the timing and magnitude of peak warmth. A
61 global average (land and ocean) surface temperature reconstruction³ from a compilation of seasonal
62 and annual-average temperature records shows a maximum of 2°C warmer temperatures during the
63 middle of the LIG. A global annual-average sea surface temperature (SST) reconstruction⁴ shows a
64 maximum of only 0.5°C warmer-than-preindustrial on a global scale that peaks during the earlier
65 LIG, but up to 1°C warmer in the high latitudes. Climate models show considerable warmth at the
66 mid-LIG, especially in the high northern latitudes, but in line with the lack of global insolation
67 forcing, little warming or even cooler conditions on a global scale⁵. At the same time, global sea level

68 during the LIG was 6-9 m higher⁶. Differences in greenhouse gas and orbital forcing over the LIG
69 relative to modern make the spatial and temporal patterns of temperature change during this period
70 distinct from what might be expected from anthropogenic warming⁷. As a result, the LIG is not an
71 analogue for future warming but offers a unique opportunity to assess the validity of earth system
72 model predictions of sea level rise in response to warming, provided that reliable paleoclimate data
73 exist for model validation⁸.

74 Sediment cores provide valuable records of changes in ocean conditions through the LIG^{4,9-11}
75 and are critical to understanding the spatiotemporal structure of temperature change. However,
76 because most available records document surface ocean conditions, deducing total ocean heat content
77 and thermosteric sea level from these records remains challenging.

78 The measurement of atmospheric noble gases trapped in glacial ice provides a method to
79 reconstruct changes in mean ocean temperature (MOT) independently from marine records¹²⁻¹⁴.
80 Changes in the relative atmospheric concentrations of krypton, xenon and nitrogen trace total ocean
81 heat content because they are caused by temperature-driven changes in gas solubilities in seawater.
82 Here, we report measurements of the ratios of Kr/N₂, Xe/N₂, and Xe/Kr in ice cores from Taylor
83 Glacier and EPICA Dome C (EDC) ice cores that cover the LIG and penultimate glacial, Marine
84 Isotope Stage 6 (MIS6, 180-136 ka). We assess the timing and magnitude of ocean temperature
85 change during the LIG and quantify the thermosteric component of elevated sea level during this
86 period.

87

88 **Last Interglacial mean ocean temperature record**

89 MOT anomalies are calculated relative to the Early Holocene (11– 10 ka) for each ice
90 core because firn fractionation corrections are more robust when calculating relative MOT change
91 compared to absolute MOT values (supplement). MOT anomalies relative to the preindustrial and
92 modern are subsequently calculated using the existing WAIS Divide¹² and EDC¹⁵ Holocene-to-
93 preindustrial MOT records and preindustrial-to-modern simulations of ocean temperature
94 change¹⁶. Based on Monte Carlo simulations that account for all known sources of uncertainty
95 (methods), we constrain peak MOT to $1.1 \pm 0.3^\circ\text{C}$ (1σ) warmer than modern at 129.0 ± 0.8 ka on
96 the Antarctic Ice Core Chronology (AICC2012)¹⁷ (Figure 1). While data for MIS6 and
97 Termination II are relatively sparse, the period of maximum MOT is highly resolved (methods).
98 Because of this and the robust age constraints from trace gas measurements for the Taylor Glacier
99 record (methods/supplement), the timing of peak MOT is well constrained.

100 The record shows a $3.4 \pm 0.5^\circ\text{C}$ MOT increase from MIS6 to the early LIG, compared to
101 the LGM to Holocene change of $2.6 \pm 0.3^\circ\text{C}$ ¹². The larger magnitude in glacial-interglacial MOT

102 change over Termination II versus Termination I is consistent with previous reconstructions of
103 deep ocean temperature during these intervals from stacks of low-resolution marine records¹¹.

104

105 **Comparison to global surface temperature records**

106 Comparison of our MOT record to stacked SST records from marine sediments⁴ over the
107 LIG reveal distinct differences between these fundamental climate parameters (Figure 2). The
108 maximum in MOT occurs earlier and exceeds the magnitude of the global SST maximum. The
109 magnitude of the peak extratropical SST anomaly agrees well with the peak MOT anomaly,
110 though the temporal evolution of each record over the LIG appears distinct. Comparison of the
111 timing of MOT and SST change is complicated by the lack of absolute age constraints for
112 sediment and ice core records spanning the LIG, and a 1-2 thousand year offset between the
113 SpeleoAge¹⁸ and AICC2012 chronologies that are applied to the SST and MOT records
114 respectively¹⁹. However, accounting for the offset in chronologies would actually increase the
115 offset in the relative timing of the MOT and global SST maxima.

116 While global SST records are good indicators of the ‘skin temperature’ and thus outgoing
117 longwave radiation for much of the planet, MOT is closely related to subsurface heat content¹⁵.
118 MOT represents volume-averaged ocean temperature, so changes in intermediate and deep ocean
119 temperatures (as opposed to SST changes) play a dominant role in setting MOT. Much of the
120 intermediate and deep ocean’s temperature is set at high latitudes via meridional circulation, so
121 the polar regions are likely crucial for the structure of MOT change, relative to that of global
122 SST²⁰.

123 MOT and Antarctic surface temperature²¹ records show strikingly similar features
124 (Figures 2 and 3). Both records are reported on AICC2012, but minor uncertainties in their
125 alignment may result from error in the Taylor Glacier chronology, or the EDC gas-ice age
126 difference²². The covariation of MOT and Antarctic temperature during the LIG follows the
127 pattern recently observed during Termination I^{12,15} in which mean ocean and high southern
128 latitude surface warming precede the increase in global SST and appear intrinsically linked. We
129 thus have strong evidence that changes in MOT outpace and exceed low latitude SST changes
130 during the LIG, which suggest that polar amplification and intermediate/deep-water formation are
131 key regulators of MOT.

132

133 **Links of MOT and ocean circulation over Termination II/LIG**

134 Recent studies have investigated the role of the bipolar seesaw, the out-of-phase
135 temperature variations between hemispheres, in the evolution of glacial terminations^{10,18,23,24}.

136 While the exact triggering mechanisms are still debated, it is generally accepted that the bipolar
137 pattern of global temperature anomalies is the result of variations in the strength of the Atlantic
138 Meridional Overturning Circulation (AMOC)²⁵. When AMOC is in a strong mode, as today, there
139 is northward heat transport at all latitudes in the Atlantic. When AMOC is weakened, this heat
140 transport is reduced, leading to a net accumulation of heat in the Southern Hemisphere.

141 A recent synthesis of available high-resolution records covering Termination II²⁶
142 including sediment records from the North Atlantic¹⁰, Chinese speleothems²⁴, and Antarctic ice
143 cores^{27,28} suggest that the AMOC was considerably weakened during Heinrich Stadial 11 (HS11,
144 ~136-129 ka), a cold period in the Northern Hemisphere that covers much of Termination II. At
145 ~129 ka, these proxy records show a rapid recovery of AMOC and Asian monsoon strength,
146 coinciding with an abrupt shift in Antarctic moisture source²⁷, CH₄ increase²⁸, and the peak in
147 MOT in our reconstruction (Figure 3). Because CH₄ and noble gases are measured on the same
148 ice samples, there is virtually no uncertainty in the relative timing of the abrupt rise in CH₄ and
149 the MOT maximum (supplement). The excellent agreement in the timing of peak MOT
150 (129.0±1.9 ka, including AICC2012 uncertainty) and the end of HS11 (128.9±0.06 ka) dated
151 from the Sanbao Cave records²⁴ also suggests an important connection between MOT and the
152 bipolar seesaw.

153 Recent modeling studies have examined the impact of reduced AMOC on surface and
154 subsurface temperature change through freshwater hosing experiments^{14,25,29}. In these simulations,
155 reduction in AMOC strength results in a globally asymmetric surface pattern of cold Northern
156 Hemisphere SSTs, as Southern Hemisphere SSTs, MOT, and Antarctica temperatures increase.
157 At the subsequent recovery of the AMOC, the accumulated subsurface heat is released, leading to
158 an abrupt increase in Northern Hemisphere SST, and gradual decrease in Southern Hemisphere
159 SST, Antarctic temperature, and MOT²⁵. This spatiotemporal pattern is consistent with the
160 observed Antarctic temperature and MOT trends during HS11 and the LIG (Figure 3). As in the
161 hosing simulations, we observe MOT and Antarctic temperature increase during the weakened
162 AMOC interval of HS11, reach a maximum at ~129 ka synchronous with AMOC recovery¹⁰, and
163 then decrease during the several thousand years following AMOC recovery. This mechanism is
164 also consistent with the lead of Southern Hemisphere over Northern Hemisphere high latitude
165 warming that is observed at the onset of the LIG^{4,9}.

166 These observations raise the question³⁰ of how much of the warmer-than-modern MOT in
167 the early LIG was due to the weakened AMOC state, and how much can be attributed to the
168 stable interglacial climate. In our record, MOT decreased and eventually stabilized by ~127 ka (at
169 latest by ~124 ka) at a temperature that is comparable to Holocene/modern MOT (+0.2±0.3°C). If

170 the observed MOT decrease was due to the release of stored heat post-AMOC recovery, then we
171 can attribute most of the MOT anomaly at the LIG onset to deglacial changes in ocean
172 circulation.

173 While our Termination II record of MOT lacks resolution at its onset, the only observed
174 warming occurs during the weakened AMOC interval, HS11. Northern Hemisphere insolation
175 forcing during Termination II exceeded that of Termination I, which may in part explain the
176 comparatively rapid disintegration of the Northern Hemisphere ice sheets during Termination II,
177 and long duration of suppressed AMOC due to strong freshwater forcing of the North Atlantic²³.
178 During Termination I the AMOC temporarily recovered, possibly due to the weaker insolation
179 and thus reduced freshwater forcing³¹. During this time, both Antarctic temperatures and MOT
180 decreased (Figure 3). The so-called ‘Antarctic Cold Reversal’, may in many ways be analogous to
181 the Antarctic and mean ocean cooling observed at the end of Termination II, post-AMOC
182 recovery. While the magnitude of MOT decrease over the Antarctic Cold Reversal was slightly
183 smaller than what is observed for the LIG onset, the net mean ocean warming during Heinrich
184 Stadial I¹² and the Younger Dryas³² of $3.4\pm 0.4^{\circ}\text{C}$ is remarkably similar to the net warming found
185 from MIS6 to the LIG peak observed in our record ($3.4\pm 0.5^{\circ}\text{C}$). In addition, the magnitude of
186 glacial-interglacial change across Termination II once MOT has stabilized is $2.5\pm 0.5^{\circ}\text{C}$, which is
187 comparable to the magnitude of MOT change across Termination I ($2.6\pm 0.3^{\circ}\text{C}$). Several studies
188 comparing Terminations I and II have posited that the larger magnitude of changes in Antarctic
189 temperature²⁷ and CO_2 ¹⁰ across Termination II are related to the delayed recovery of AMOC
190 strength. Our record suggests the same is true for MOT.

191 These observations suggest that the AMOC interruptions during the past two terminations
192 transiently provided an additional $\sim 1^{\circ}\text{C}$ of mean ocean warming above the net glacial-interglacial
193 MOT change. A recent quantitative assessment of Earth’s radiative imbalance over Termination
194 I¹⁵ found maxima in positive radiative imbalance during the Younger Dryas and Heinrich Stadial
195 I, suggesting that reduced AMOC during these intervals contributed energy to the climate system
196 through an increase in ocean heat storage. This storage and subsequent release of energy may
197 play a critical role in terminations²⁹. As shown in simulations²⁹, when the AMOC is reduced the
198 subsurface ocean works as a ‘capacitor’, storing heat while the surface (centered on the North
199 Atlantic) remains cold. Once the AMOC recovers, the subsurface heat is released, providing
200 enhanced surface warming. While our MOT record lacks the necessary resolution to conduct a
201 similar assessment of radiative imbalance across Termination II, the comparable magnitudes of
202 enhanced mean ocean warming during weakened AMOC intervals over the last two terminations
203 suggest that this mechanism was also important for Termination II. Along with the potential

204 importance of AMOC interruptions in releasing Southern Ocean CO₂^{33,34} and destabilizing
205 Northern Hemisphere ice sheets^{35,36}, their role in providing additional energy to the climate
206 system lends support to the hypothesis that AMOC interruptions are not merely incidental to
207 terminations, but play a role in driving the climate out of glacial conditions^{18,24}.

208

209 **Implications for West Antarctic Ice Sheet stability**

210 The MOT changes across the LIG have direct and indirect implications for sea level.
211 Pinning down the sources contributing to the LIG global mean sea level highstand is crucial to
212 understand the vulnerability of modern ice sheets to global warming. From CMIP5 estimates of
213 the expansion efficiency of heat (0.12 m YJ⁻¹)³⁷, we find that the 1.1±0.3°C MOT anomaly during
214 the early stages of the LIG contributed 0.7±0.3m to elevated sea level. By ~127 ka MOT had
215 decreased to near-modern values, and no appreciable thermosteric contribution (relative to
216 modern) is expected by this early stage in the interglacial. In fact, our record implies a trend of
217 thermosteric sea level lowering in the first several thousand years of the LIG. Coral reef records
218 indicate that sea level was already 5.9±1.7m higher than modern at 128.6±0.8ka³⁸, requiring a
219 substantial ice sheet (in addition to the thermosteric) contribution early in the LIG to explain this
220 magnitude of elevated sea level.

221 The early maximum in MOT may have played another, more indirect role in contributing
222 to sea level rise during the LIG. In recent Antarctic Ice Sheet simulations of the LIG^{39,40}, ocean
223 warming played an important role in mass loss from the West Antarctic Ice Sheet. Ref. 50 found
224 that if ocean warming occurred shortly after the glacial termination, the West Antarctic Ice Sheet
225 was more prone to lose mass because of enhanced reverse-sloped beds at grounding lines. By
226 invoking sub-shelf melting through Southern Ocean warming, ref. 51 derived the highest rates of
227 sea level rise during maximum Antarctic temperatures at the end of Termination II, synchronous
228 to our MOT maximum. The delay in AMOC recovery and resulting accumulation of heat in the
229 ocean interior and Southern Hemisphere at the end of Termination II may therefore have played
230 an important role in West Antarctic Ice Sheet mass loss and elevated sea level during the LIG.

231 An important caveat to consider for this hypothesis is that MOT is not a proxy for ocean
232 temperatures directly under ice shelves, and higher MOT does not necessarily imply that
233 temperatures in vulnerable sub-ice shelf regions were enhanced. However, MOT and the
234 temperature of circumpolar deep water are intrinsically linked because circumpolar deep water is
235 made up of a representative mixture of waters from all ocean basins⁴¹ and is brought efficiently to
236 the surface by isopycnal mixing in the Southern Ocean. If, as today, circumpolar deep water

237 intruded onto the Antarctic continental shelf, its ice melting capacity would be enhanced during
238 the early stages of the LIG.

239

240 **Conclusions**

241 The ocean heat anomaly provided from our MOT reconstruction is a simple but important
242 metric to evaluate in earth system models, making it useful for forthcoming simulations of the
243 LIG. Comparison with other proxy and model results suggest that peak MOT coincided with the
244 abrupt recovery of the AMOC at the end of Termination II and was a transient rather than stable
245 feature of the LIG. Enhanced MOT contributed to elevated thermohaline sea level during the early
246 stages of the LIG and may have played a more indirect role in the sea level highstand through
247 amplified melting of ice sheets and shelves from below. The temporal evolution of AMOC and
248 MOT over the past two terminations suggest that the ocean's overturning circulation plays a
249 dominant role in controlling the timing and magnitude of MOT change across terminations;
250 studying the LIG in the context of the termination that preceded it provides a more complete view
251 of the climate evolution that occurred over this interval.

252

253

254

255

256

257

258

259 **References**

- 260 1. Stocker, T. F. *et al.* Climate change 2013: The physical science basis. (2013).
- 261 2. Pritchard, H. D. *et al.* Antarctic ice-sheet loss driven by basal melting of ice shelves.
262 *Nature* **484**, 502–505 (2012).
- 263 3. Snyder, C. W. Evolution of global temperature over the past two million years. *Nature*
264 **538**, 226–228 (2016).
- 265 4. Hoffman, J. S., Parnell, A. C. & He, F. Regional and global sea-surface temperatures
266 during the last interglaciation. *Science* **279**, 276–279 (2017).
- 267 5. Otto-Bliesner, B. L. *et al.* How warm was the last interglacial? New model – data
268 comparisons. *Philos. Trans. R. Soc. A* **371**, (2013).
- 269 6. Kopp, R. E., Simons, F. J., Mitrovica, J. X., Maloof, A. C. & Oppenheimer, M.
270 Probabilistic assessment of sea level during the last interglacial stage. *Nature* **462**, 863–
271 867 (2009).
- 272 7. Masson-Delmotte, V. *et al.* Sensitivity of interglacial Greenland temperature and
273 $\delta^{18}\text{O}$: ice core data, orbital and increased CO₂ climate simulations. *Clim. Past* **7**,
274 1041–1059 (2011).
- 275 8. Fischer, H. *et al.* Palaeoclimate constraints on the impact of 2°C anthropogenic warming

- 276 and beyond. *Nat. Geosci.* **11**, 475–485 (2018).
- 277 9. Capron, E. *et al.* Temporal and spatial structure of multi-millennial temperature changes at
278 high latitudes during the Last Interglacial. *Quat. Sci. Rev.* **103**, 116–133 (2014).
- 279 10. Deaney, E. L., Barker, S. & Flierdt, T. Van De. Timing and nature of AMOC recovery
280 across Termination 2 and magnitude of deglacial CO₂ change. *Nat. Commun.* **8**, 1–10
281 (2017).
- 282 11. Shakun, J. D., Lea, D. W., Lisiecki, L. E. & Raymo, M. E. An 800-kyr record of global
283 surface ocean δ 18 O and implications for ice volume-temperature coupling. *Earth Planet.*
284 *Sci. Lett.* **426**, 58–68 (2015).
- 285 12. Bereiter, B., Shackleton, S., Baggenstos, D., Kawamura, K. & Severinghaus, J. Mean
286 global ocean temperatures during the last glacial transition. *Nature* **553**, 39–44 (2018).
- 287 13. Headly, M. A. & Severinghaus, J. P. A method to measure Kr/N₂ ratios in air bubbles
288 trapped in ice cores and its application in reconstructing past mean ocean temperature. *J.*
289 *Geophys. Res.* **112**, 1–12 (2007).
- 290 14. Ritz, S. P., Stocker, T. F. & Severinghaus, J. P. Noble gases as proxies of mean ocean
291 temperature : sensitivity studies using a climate model of reduced complexity. *Quat. Sci.*
292 *Rev.* **30**, 3728–3741 (2011).
- 293 15. Baggenstos, D. *et al.* The Earth’s radiative imbalance from the Last Glacial Maximum to
294 the present. *Proc. Natl. Acad. Sci.* **116**, 14881–14886 (2019).
- 295 16. Gebbie, G. & Huybers, P. The Little Ice Age and 20th-century deep Pacific cooling.
296 *Science* **363**, 70–74 (2019).
- 297 17. Bazin, L. *et al.* An optimized multi-proxy, multi-site Antarctic ice and gas orbital
298 chronology (AICC2012): 120-800 ka. *Clim. Past* **9**, 1715–1731 (2013).
- 299 18. Barker, S. *et al.* 800,000 Years of Abrupt Climate Variability. *Science* **334**, 347–352
300 (2011).
- 301 19. Capron, E., Govin, A., Feng, R., Otto-Bliesner, B. L. & Wolff, E. W. Critical evaluation
302 of climate syntheses to benchmark CMIP6 / PMIP4 127 ka Last Interglacial simulations in
303 the high-latitude regions. *Quat. Sci. Rev.* **168**, 137–150 (2017).
- 304 20. Gebbie, G. & Huybers, P. How is the ocean filled ? *Geophys. Res. Lett.* **38**, (2011).
- 305 21. Jouzel, J. *et al.* Orbital and Millennial Antarctic Climate Variability over the Past 800,000
306 years. *Science* **317**, 793–796 (2007).
- 307 22. Parrenin, F. *et al.* On the gas-ice depth difference (Δ depth) along the EPICA Dome C ice
308 core. *Clim. Past* **8**, 1239–1255 (2012).
- 309 23. Marino, G. *et al.* Bipolar seesaw control on last interglacial sea level. *Nature* **522**, 197–
310 201 (2015).
- 311 24. Cheng, H. *et al.* Ice Age Terminations. *Science* **326**, 248–252 (2009).
- 312 25. Pedro, J. B. *et al.* Beyond the bipolar seesaw: Toward a process understanding of
313 interhemispheric coupling. *Quat. Sci. Rev.* **192**, 27–46 (2018).
- 314 26. Menviel, L. *et al.* The penultimate deglaciation: protocol for PMIP4 transient numerical
315 simulations between 140 and 127 ka , version 1.0. *Geosci. Model Dev. Discuss.* (2019).
- 316 27. Masson-Delmotte, V. *et al.* Abrupt change of Antarctic moisture origin at the end of
317 Termination II. *Proc. Natl. Acad. Sci.* **107**, 10–13 (2010).
- 318 28. Loulergue, L. *et al.* Orbital and millennial-scale features of atmospheric CH₄ over the past
319 800,000 years. *Nature* **453**, 383–386 (2008).
- 320 29. Galbraith, E. D., Merlis, T. M. & Palter, J. B. Destabilization of glacial climate by the
321 radiative impact of Atlantic Meridional Overturning Circulation disruptions. *Geophys.*
322 *Res. Lett.* **43**, 8214–8221 (2016).
- 323 30. Barker, S. *et al.* Early interglacial legacy of deglacial climate instability. *Paleoceanogr.*
324 *Paleoclimatology* (2019). doi:10.1029/2019PA003661
- 325 31. Carlson, A. E. Why there was not a Younger Dryas-like event during the Penultimate
326 Deglaciation. *Quat. Sci. Rev.* **27**, 882–887 (2008).

- 327 32. Shackleton, S. *et al.* Is the Noble Gas-Based Rate of Ocean Warming During the Younger
328 Dryas Overestimated? *Geophys. Res. Lett.* **46**, (2019).
- 329 33. Anderson, R. F. *et al.* Wind-driven upwelling in the southern ocean and the deglacial rise
330 in atmospheric CO₂. *Science* **323**, 1443–1448 (2009).
- 331 34. Toggweiler, J. R., Russell, J. L. & Carson, S. R. Midlatitude westerlies, atmospheric CO₂,
332 and climate change during the ice ages. *Paleoceanography* **21**, 1–15 (2006).
- 333 35. Marcott, S. A. *et al.* Ice-shelf collapse from subsurface warming as a trigger for Heinrich
334 events. *Proc. Natl. Acad. Sci.* **108**, 13415 LP – 13419 (2011).
- 335 36. Bassis, J. N., Peterson, S. V & Cathles, L. Mac. Heinrich events triggered by ocean
336 forcing and modulated by isostatic adjustment. *Nature* **542**, 332–334 (2017).
- 337 37. Kuhlbrodt, T. & Gregory, J. M. Ocean heat uptake and its consequences for the magnitude
338 of sea level rise and climate change. *Geophys. Res. Lett.* **39**, 1–6 (2012).
- 339 38. Dutton, A., Webster, J. M., Zwartz, D. & Lambeck, K. Tropical tales of polar ice:
340 evidence of Last Interglacial polar ice sheet retreat recorded by fossil reefs of the granitic
341 Seychelles islands. *Quat. Sci. Rev.* **107**, 182–196 (2015).
- 342 39. Pollard, D. & Deconto, R. M. Contribution of Antarctica to past and future sea-level rise.
343 *Nature* **531**, 591–597 (2016).
- 344 40. Sutter, J., Gierz, P., Grosfeld, K., Thoma, M. & Lohmann, G. Ocean temperature
345 thresholds for Last Interglacial West Antarctic Ice Sheet collapse. *Geophys. Res. Lett.* **43**,
346 2675–2682 (2016).
- 347 41. Elderfield, H. *et al.* Evolution of Ocean Temperature and Ice Volume Through the Mid-
348 Pleistocene Climate Transition. *Science* **337**, (2012).
- 349 42. Lisiecki, L. E. & Raymo, M. E. A Pliocene-Pleistocene stack of 57 globally distributed
350 benthic δ¹⁸O records. *Paleoceanography* **20**, (2005).
- 351 43. Schneider, R., Schmitt, J., Köhler, P., Joos, F. & Fischer, H. A reconstruction of
352 atmospheric carbon dioxide and its stable carbon isotopic composition from the
353 penultimate glacial maximum to the last glacial inception. *Clim. Past* **9**, 2507–2523
354 (2013).
- 355 44. Wang, Y. *et al.* Millennial- and orbital-scale changes in the East Asian monsoon over the
356 past 224,000 years. *Nature* **451**, 1090–1093 (2008).
- 357 45. Grant, K. M. *et al.* Sea-level variability over five glacial cycles. *Nat. Commun.* **5**, 1–9
358 (2014).
- 359 46. Marcott, S. A. *et al.* Centennial-scale changes in the global carbon cycle during the last
360 deglaciation. *Nature* **514**, 616–619 (2014).
- 361 47. Buizert, C. *et al.* Precise inter-polar phasing of abrupt climate change during the last ice
362 age. *Nature* **520**, 661–665 (2015).
- 363 48. Buizert, C. *et al.* The WAIS-Divide deep ice core WD2014 chronology – Part 1 : Methane
364 synchronization (68 – 31 ka BP) and the gas age-ice age difference. *Clim. Past* **11**, 153
365 (2015).
- 366 49. Dykoski, C. A. *et al.* A high-resolution, absolute-dated Holocene and deglacial Asian
367 monsoon record from Dongge Cave, China. *Earth Planet. Sci. Lett.* **233**, 71–86 (2005).
- 368 50. Wang, Y. *et al.* A high-resolution absolute-dated late pleistocene monsoon record from
369 Hulu Cave, China. *Science* **294**, 2345–2348 (2001).
- 370 51. Roberts, N. L., Piotrowski, A. M., McManus, J. F. & Keigwin, L. D. Synchronous
371 Deglacial Overturning and Water Mass Source Changes. *Science* **327**, 75–78 (2010).
- 372 52. Lambeck, K., Rouby, H., Purcell, A., Sun, Y. & Sambridge, M. Sea level and global ice
373 volumes from the Last Glacial Maximum to the Holocene. *Proc. Natl. Acad. Sci.* **111**,
374 15296–15303 (2014).
- 375

376 **Corresponding Author**

377 Correspondence and request for materials should be addressed to S.S. at sshackle@ucsd.edu.

378

379 **Acknowledgements**

380

381 This research was supported by NSF grants 1246148 (SIO), 1245821 (OSU) and 1245659 (UR).
382 We thank Kathy Schroeder, Mike Jayred, Peter Sperlich, Isaac Vimont, Jacob Ward, Heidi Roop,
383 Peter Neff, and Andrew Smith for their invaluable field support for this project. Ice Drilling
384 Design and Operations (IDDO) provided drilling support, and the US Antarctic Program provided
385 logistical support for this project. Thanks to Ross Beaudette for lab support at SIO, to Michael
386 Kalk for CO₂ measurements at OSU, and to Monica Arienzo and Nathan Chellman for their
387 heroic operation of the continuous melting system at DRI. The research at University of Bern
388 leading to these results has received funding from the European Research Council (ERC) under
389 the European Union's Seventh Framework Programme FP7/2007-2013 ERC Grant 226172 (ERC
390 Advanced Grant Modern Approaches to Temperature Reconstructions in polar Ice Cores
391 (MATRICs)) and the Swiss national Science Foundation (200020_172506 (iCEP),
392 200021_155906 (NOTICE)). The EDC samples were obtained under the framework of EPICA, a
393 joint European Science Foundation/European Commission scientific program funded by the
394 European Union and national contributions from Belgium, Denmark, France, Germany, Italy, the
395 Netherlands, Norway, Sweden, Switzerland, and the United Kingdom. The main logistic support
396 was provided by IPEV and PNRA at Dome C.

397

398 **Author Contributions**

399

400 J.P.S. and S.S. designed research. S.S., M.H., D.B., and T.K. performed noble gas measurements.
401 J.A.M., E.J.B., R.H.R., J.R.M. and S.S. performed trace gas field/lab measurements for Taylor
402 Glacier age model. S.S., D.B., J.A.M., M.N.D., B.B., T.K.B., R.H.R., E.J.B., V.V.P., M.J.R., T.K.,
403 M.H., J.S., H.F., and J.P.S. analyzed data. S.S. wrote the paper with input from all authors.

404

405 **Competing Interests**

406 The authors declare no competing interests.

407

408

409 **Figure Captions**

410

411 **Figure 1. Mean Ocean Temperature (MOT) anomaly from Kr/N₂, Xe/N₂, and Xe/Kr.** MOT
412 data is shown with 1 σ error (methods). Vertical dashed lines mark the Marine Isotope Stage 6
413 (MIS6), Heinrich Stadial 11 (HS11) and Last Interglacial (LIG) boundaries. Gray bars indicate
414 the time intervals for which MIS6 MOT (>136 ka), peak MOT (129.0 \pm 0.8 ka), and stable LIG
415 MOT (<127 ka) are calculated. MOT is reported on the AICC2012¹⁷ chronology. Global average
416 deep ocean temperature (DOT) from stacked marine sediment records¹¹ on LR04⁴² is shown for
417 reference.

418

419

420 **Figure 2. Surface and mean ocean temperature (MOT) anomalies during the LIG.** **a)** global
421 and **b)** extratropical sea surface temperatures (SST) (relative to preindustrial) from the Northern
422 Hemisphere (red) and Southern Hemisphere (blue) from stacked SST proxy records⁴ on the
423 SpeleoAge chronology¹⁸. Shading shows 2 σ confidence interval. **c)** MOT (relative to modern) on

424 AICC2012¹⁷ with 1 σ error bars (points) and 1 σ confidence envelope (shading). **d**) EPICA Dome
425 C (EDC) surface air temperature²¹ (SAT, relative to average of last 1000 years) on AICC2012.

426

427 **Figure 3. Climate records of Terminations II and I.** Left panel: climate records of Termination
428 II. **a**) Mean ocean temperature (MOT) anomaly relative to modern from this study with 1 σ error
429 (shading). **b**) Antarctic temperature²¹ anomaly relative to average of last 1000 years, **c**) CO₂⁴³, and
430 **d**) CH₄²⁸. Green points show Taylor Glacier CH₄ measurements. a)-d) are presented on
431 AICC2012¹⁷. **e**) Sanbao^{24,44} ²³⁰Th-dated $\delta^{18}\text{O}_{\text{calcite}}$ records. Colors distinguish individual
432 speleothems. **f**) North Atlantic ϵNd^{10} on core-specific age scale. **g**) Red Sea Level anomaly
433 corrected for isostatic effects⁴⁵ on core-specific age scale (light blue). Gray diamonds show coral
434 reef sea level records³⁸. **h**) Summer solstice insolation at 65°N. Right panel: climate records of
435 Termination I with differences from left panel as follows. **a**) MOT anomaly relative to modern
436 from WAIS Divide¹² (turquoise) and Taylor Glacier³² (dark blue). Error bars show spread (1 σ) of
437 replicate samples measured at SIO for this study (supplement). **c**) CO₂⁴⁶, and **d**) CH₄⁴⁷. a), c) and
438 d) are presented on WD2014⁴⁸. **e**) Dongge⁴⁹ (red) and Hulu⁵⁰ (orange and yellow) $\delta^{18}\text{O}_{\text{calcite}}$
439 records. **f**) North Atlantic ϵNd^{51} on core-specific age scale **g**) eustatic sea level⁵² with 1 σ error
440 from radiocarbon/uranium-series dated coral and sediment records. Orange bars indicate times
441 when AMOC was in a weakened mode and blue bars show periods of strong AMOC and mean
442 ocean/Antarctic cooling. Top panel: benthic $\delta^{18}\text{O}$ on LR04⁴². Gray bars highlight the intervals
443 shown in the panels below.

444

445

446

446 **Methods**

447

448 **Taylor Glacier sampling and site description**

449

450 Taylor Glacier is an outlet glacier of the East Antarctic Ice Sheet with a >80 km long
451 ablation zone exposing easily accessible old ice at the surface. Its accumulation zone is located on
452 the northern flank of Taylor Dome and it terminates in Taylor Valley. Extensive work on
453 mapping the stratigraphy of the glacier identified ice from the LIG located near the terminus of
454 the glacier^{53–55}.

455 For this study, a total of four large-diameter ice cores were collected during the 2014/15
456 and 2015/16 Antarctic field seasons (Figure S1 in supplement). Two cores spanning
457 approximately 155 – 120 ka were collected approximately 4 km from the glacier terminus.
458 Additionally, two cores were drilled along a previously-established across-flow transect⁵³ from
459 the early Holocene (10.6 ka) and Last Glacial Maximum (LGM, 19.9 ka) to serve as a
460 comparison to LIG and MIS6 MOT samples. Cores were drilled with the Blue Ice Drill⁵⁶ and are
461 24.1 cm in diameter. Cores were processed and subdivided in the field and analyzed for noble
462 gases for MOT reconstruction as well as other atmospheric gases used to establish the chronology
463 of the record.

464

465 **Taylor Glacier core chronology**

466

467 A major challenge in sampling a blue ice area is establishing ages for the samples⁵⁷. Ice
468 from Taylor Glacier has traveled tens of kilometers from its deposition site and has likely
469 undergone non-uniform thinning and folding. While the dynamics of the glacier have been
470 studied in detail^{58,59}, not enough is known about the basal topography or subsurface ice flow to
471 build a chronology for the glacier from a glaciological model.

472 We therefore use alternative methods to construct the chronology for our samples.
473 Previous work in blue ice areas^{53,60–62} has demonstrated success in establishing ice sample
474 chronologies through value and/or inflection point matching of well-mixed atmospheric gases to

475 well-dated ice core records⁶³. For this study the chronology was constructed using a least-squares
476 fitting method with measurements of methane concentrations (CH₄), molecular oxygen isotopic
477 composition ($\delta^{18}\text{O}_{\text{atm}}$), and carbon dioxide concentrations (CO₂), tied to EPICA Dome C (EDC)
478 reference records^{28,43,64} on the Antarctic Ice Core Chronology (AICC2012)^{17,65}. This method
479 allows for a construction of an age probability distribution for each noble gas sample that can be
480 used to assess sample age uncertainty (supplement).

481

482 **Taylor Glacier noble gas measurements**

483

484 Taylor Glacier measurements of noble gases for MOT reconstruction were made at
485 Scripps Institution of Oceanography (SIO). A total of 45 ice samples from the 2014/15 and
486 2015/16 cores were analyzed, including eight replicate samples, giving 37 unique MOT samples.
487 Of the 45 samples, 3 were rejected due to sample age uncertainty (see supplement). In addition, at
488 SIO and Bern five samples from the Holocene (10.6 ka) and five from the LGM (19.9 ka) were
489 measured (Figure 3) at each institution. The motivation for this analysis was to verify the quality
490 of the noble gas records by comparison to published MOT records¹², and to verify that any offsets
491 in the EDC and Taylor Glacier MOT results were unrelated to lab offsets (see supplementary
492 materials).

493 The analytical methods for noble gas measurements are described in detail by Bereiter et
494 al. (2018b). In short, ~800 grams of ice were melted under vacuum and liberated gases (~80 ml at
495 standard temperature and pressure, STP) were cryogenically trapped in stainless steel dip tubes.
496 After gas extraction, the samples were split into two aliquots. The larger (~78 ml STP) aliquot
497 was exposed to a Zr/Al alloy at 900°C to remove all non-noble gases and measured on a Thermo-
498 Finnigan MAT-253 isotope ratio mass spectrometer via dual inlet method for ⁴⁰Ar/³⁸Ar ($\delta^{40/38}\text{Ar}$),
499 ⁴⁰Ar/³⁶Ar ($\delta^{40/36}\text{Ar}$), ⁸⁶Kr/⁸⁴Kr ($\delta^{86/84}\text{Kr}$), ⁸⁶Kr/⁸³Kr ($\delta^{86/83}\text{Kr}$), ⁸⁶Kr/⁸²Kr ($\delta^{86/82}\text{Kr}$), ⁸⁴Kr/⁴⁰Ar
500 ($\delta\text{Kr}/\text{Ar}$), and ¹³²Xe/⁴⁰Ar ($\delta\text{Xe}/\text{Ar}$). The smaller aliquot (~2 ml, STP) was passed through a
501 cryotrap (-196°C) to remove CO₂ and measured on a Thermo-Finnigan MAT Delta V isotope
502 ratio mass spectrometer via dual inlet method for ²⁹N₂/²⁸N₂ ($\delta^{15}\text{N}$), ³⁴O₂/³²O₂ ($\delta^{18}\text{O}$), ³²O₂/²⁸N₂
503 ($\delta\text{O}_2/\text{N}_2$), and ⁴⁰Ar/²⁸N₂ ($\delta\text{Ar}/\text{N}_2$). Measurements were corrected for pressure imbalance and
504 chemical slope according to established procedure⁶⁷.

505 All data are reported in delta notation, relative to a modern atmosphere standard. Because
506 argon is preferentially lost relative to xenon and krypton during ice bubble formation⁶⁸, we
507 mathematically combine $\delta\text{Xe}/\text{Ar}$, $\delta\text{Kr}/\text{Ar}$, and $\delta\text{Ar}/\text{N}_2$ to obtain $\delta\text{Kr}/\text{N}_2$, $\delta\text{Xe}/\text{N}_2$, and $\delta\text{Xe}/\text{Kr}$.

508

509 **Taylor Glacier fractionation corrections**

510

511 To reconstruct ocean temperature from Kr/N₂, Xe/N₂ and Xe/Kr, it is necessary to correct
512 for fractionation during firnification, the process by which fresh snow compacts, transitioning to
513 denser firn and eventually to glacial ice containing air trapped in bubbles. While the free
514 troposphere is well mixed through convective processes, the low permeability of the firn restricts
515 bulk flow; gases within the firn column are transported primarily via molecular diffusion⁶⁹. This
516 allows for gravitational settling and thermal diffusion to alter firn air from its atmospheric
517 composition before it is occluded in glacial ice^{70,71}. As such, Kr/N₂, Xe/N₂ and Xe/Kr must be
518 corrected for fractionating processes to derive the paleoatmospheric composition for inferring
519 MOT.

520 As suggested by ref. 12, under/over-correction of fractionation may lead to systematic
521 offsets in MOT, but the effect primarily impacts the absolute MOT anomaly (relative to modern)
522 and has little impact on relative MOT change within a record. We investigate the influence of the
523 choice in methods of fractionation correction on the MOT record and find that different methods
524 shift the absolute MOT record up or down but have little effect on relative MOT change in the

525 Taylor Glacier record (see supplement). We thus compute the MOT anomalies relative to the
526 Taylor Glacier Holocene (10.6 ka) samples and then estimate the Holocene – modern MOT
527 difference (and uncertainties) from the WAIS Divide MOT record and model simulations of
528 ocean heat content over the last 2000 years¹⁶. A detailed description and assessment of the
529 fractionation corrections is included in the supplementary materials.

530

531 **EDC ice core noble gas analysis**

532

533 Four EDC ice core samples from the LIG and four from MIS6 were analyzed at the
534 University of Bern and included in this study. Measurement and data processing for these
535 samples are similar to the analysis of Taylor Glacier samples with a few important distinctions
536 (ref. 15 and supplement). Chronological uncertainties are not considered in this analysis, because
537 the Taylor Glacier chronology is tied to that of EDC through ice core synchronization and
538 contribute minimally to the total uncertainty for these samples. In addition, the approach to firm
539 fractionation corrections differs slightly between Taylor Glacier and EDC (supplementary section
540 SI4).

541

542 **Derivation of MOT from noble gas data**

543

544 To reconstruct MOT values from fractionation-corrected Kr/N₂, Xe/N₂ and Xe/Kr, we use
545 the ocean-atmosphere box model of ref. 12 with several modifications. We make no assumptions
546 about the glacial-interglacial change in the ocean saturation state and use current estimates of
547 krypton and xenon undersaturation⁷² in the box model for the entirety of the record. We also do
548 not invoke the glacial-interglacial changes in the relative water mass distributions that were
549 applied in ref. 12 and use the modern distributions of Antarctic Bottom Water and North Atlantic
550 Deep Water to derive MOT over the full record.

551 We account for the effects of changes in ocean salinity, volume, and atmospheric
552 pressure on the oceanic inventories of krypton, xenon and nitrogen using the sea level record of
553 ref. 34 corrected for isostatic effects (supplement). We also include the influence of the large ice
554 shelf over the Arctic during MIS6, which holds the equivalent of 15 meters of sea level,
555 influencing ocean salinity and volume, but not sea level⁷³.

556 To assess uncertainty in our MOT record we run 10,000 Monte Carlo simulations of our
557 reconstruction with all known analytical and dating uncertainties in the MOT and sea level
558 records, as well as the uncertainty in the Holocene-to-modern MOT change. We include
559 uncertainties in measured Kr/N₂, Xe/N₂ and Xe/Kr and the isotope data used to correct for firm
560 processes in our simulations, as well as the method used for fractionation corrections
561 (supplementary section SI4). To account for age uncertainties in the MOT record, we use an
562 inverse transform method⁷⁴ to randomly sample from our age probability distribution to include in
563 our Monte Carlo simulations. For our final uncertainty estimate, we use the average of the three
564 MOT records (and the Monte Carlo simulations) from Kr/N₂, Xe/N₂ and Xe/Kr to minimize the
565 influence of analytical noise from any single measurement.

566 The 1 σ confidence envelope shown in Figures 2 and 3 was constructed using the
567 MATLAB cubic smoothing spline function (csaps) with a 2500 year cut off period on the 10,000
568 Monte Carlo MOT reconstructions. Each reconstruction was resampled using a bootstrapping
569 method before the spline was produced. The 1 σ confidence envelope was then calculated from
570 the distribution of the Monte Carlo splines at each time interval in the record.

571

572 **Data availability**

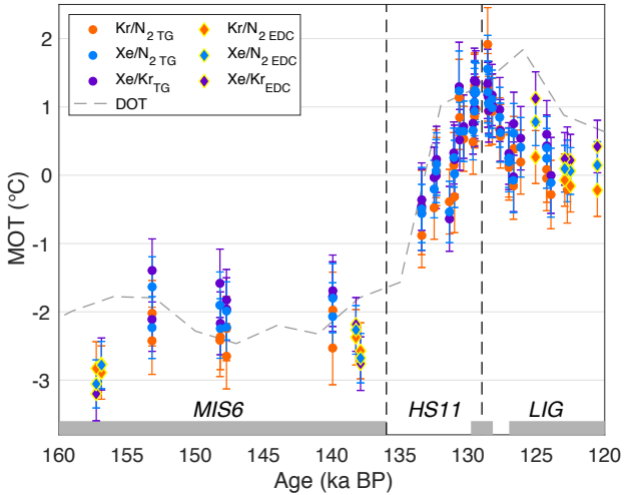
573 Presented data are available online at <http://www.usap-dc.org/view/dataset/601218>.

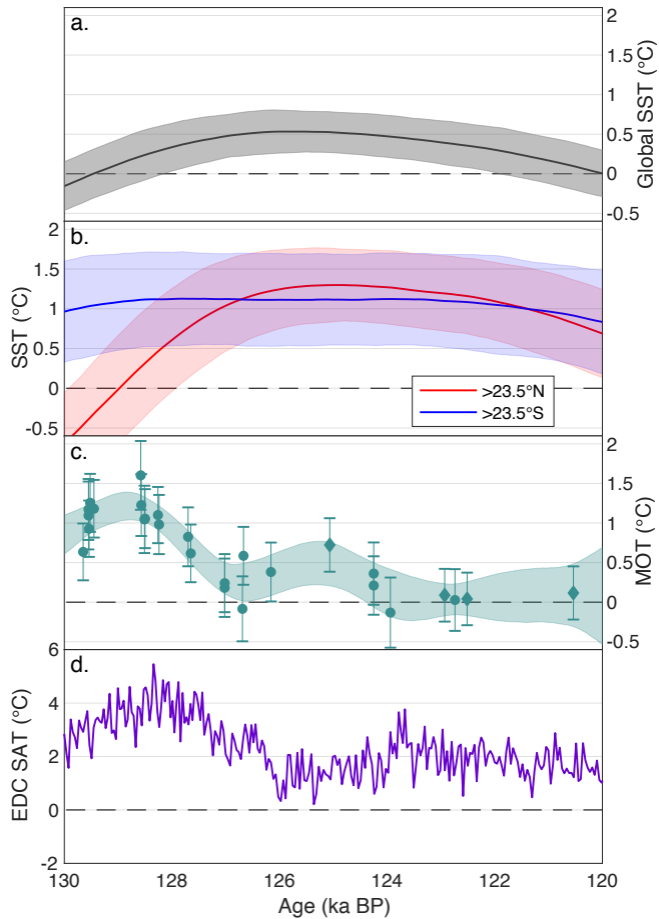
574

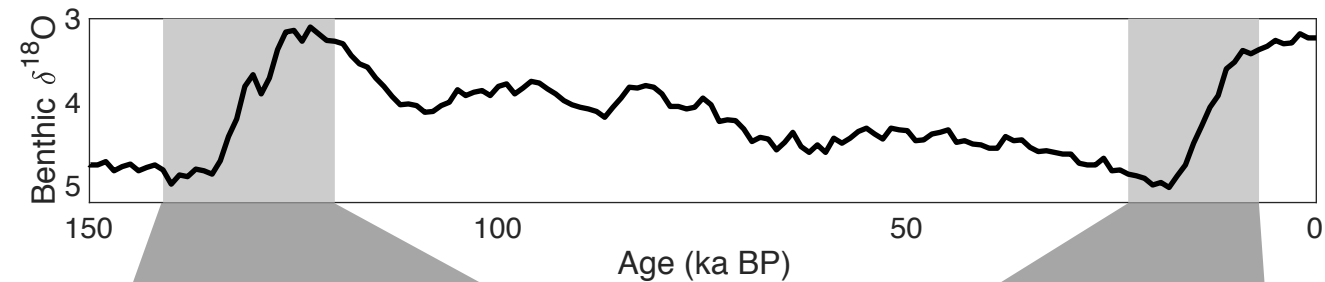
575 **References**

- 576
577 53. Baggenstos, D. *et al.* Atmospheric gas records from Taylor Glacier, Antarctica, reveal
578 ancient ice with ages spanning the entire last glacial cycle. *Clim. Past* **13**, 943–958 (2017).
579 54. Buizert, C. *et al.* Radiometric ⁸¹Kr dating identifies 120,000-year-old ice at Taylor
580 Glacier, Antarctica. *Proc. Natl. Acad. Sci.* **111**, 6876–6881 (2014).
581 55. Aarons, S. M., Aciego, S. M., McConnell, J. R., Delmonte, B. & Baccolo, G. Dust
582 transport to the Taylor Glacier, Antarctica during the last interglacial. *Geophys. Res. Lett.*
583 **46**, 2261–2270 (2019).
584 56. Kuhl, T. W. *et al.* A new large-diameter ice-core drill: The Blue Ice Drill. *Ann. Glaciol.*
585 **55**, 1–6 (2014).
586 57. Bintanja, R. On the glaciological, meteorological, and climatological significance of
587 Antarctic blue ice areas. *Rev. Geophys.* **37**, 337–359 (1999).
588 58. Aciego, S. M., Cuffey, K. M., Kavanaugh, J. L., Morse, D. L. & Severinghaus, J. P.
589 Pleistocene ice and paleo-strain rates at Taylor Glacier, Antarctica. *Quat. Res.* **68**, 303–
590 313 (2007).
591 59. Kavanaugh, J. L. & Cuffey, K. M. Dynamics and mass balance of Taylor Glacier,
592 Antarctica: 2. Force balance and longitudinal coupling. *J. Geophys. Res.* **114**, (2009).
593 60. Petrenko, V. V., Severinghaus, J. P., Brook, E. J., Reeh, N. & Schaefer, H. Gas records
594 from the West Greenland ice margin covering the Last Glacial Termination : a horizontal
595 ice core. *Quat. Sci. Rev.* **25**, 865–875 (2006).
596 61. Bauska, T. K. *et al.* Carbon isotopes characterize rapid changes in atmospheric carbon
597 dioxide during the last deglaciation. *Proc. Natl. Acad. Sci.* **113**, 3465–3470 (2016).
598 62. Menking, J. A. *et al.* Spatial pattern of accumulation at Taylor Dome during Marine
599 Isotope Stage 4 : stratigraphic constraints from Taylor Glacier. *Clim. Past* **15**, 1537–1556
600 (2019).
601 63. Blunier, T. *et al.* Synchronization of ice core records via atmospheric gases. *Clim. Past* **3**,
602 325–330 (2007).
603 64. Landais, A. *et al.* Two-phase change in CO₂, Antarctic temperature and global climate
604 during Termination II. *Nat. Geosci.* **6**, 1062–1065 (2013).
605 65. Veres, D. *et al.* The Antarctic ice core chronology (AICC2012): an optimized for the last
606 120 thousand years. *Clim. Past* **9**, 1733–1748 (2013).
607 66. Bereiter, B., Kawamura, K. & Severinghaus, J. P. New methods for measuring
608 atmospheric heavy noble gas isotope and elemental ratios in ice core samples. *Rapid*
609 *Commun. Mass Spectrom.* **32**, 801–814 (2018).
610 67. Severinghaus, J. P., Grachev, A., Luz, B. & Caillon, N. A method for precise
611 measurement of argon ⁴⁰/₃₆ and krypton/argon ratios in trapped air in polar ice with
612 applications to past firn thickness and abrupt climate change in Greenland and at Siple
613 Dome , Antarctica. *Geochim. Cosmochim. Acta* **67**, 325–343 (2003).
614 68. Severinghaus, J. P. & Battle, M. O. Fractionation of gases in polar ice during bubble
615 close-off: New constraints from firn air Ne, Kr and Xe observations. *Earth Planet. Sci.*
616 *Lett.* **244**, 474–500 (2006).
617 69. Schwander, J., Stauffer, B. & Sigg, A. Air mixing in firn and the age of the air at pore
618 close-off. *Ann. Glaciol.* **10**, 141–145 (1988).
619 70. Schwander, J. The transformation of snow to ice and the occlusion of gases. in *The*
620 *Environmental Record in Glaciers and Ice Sheets* (eds. Oeschger, H. & Langway, C. C.)
621 53–67 (1989).
622 71. Severinghaus, J. P., Sowers, T., Brook, E. J., Alley, R. B. & Bender, M. L. Timing of
623 abrupt climate change at the end of the Younger Dryas interval from thermally
624 fractionated gases in polar ice. *Nature* **391**, 141–146 (1998).
625 72. Hamme, R. C. & Severinghaus, J. P. Trace gas disequilibria during deep-water formation.
626 *Deep Sea Res.* **54**, 939–950 (2007).

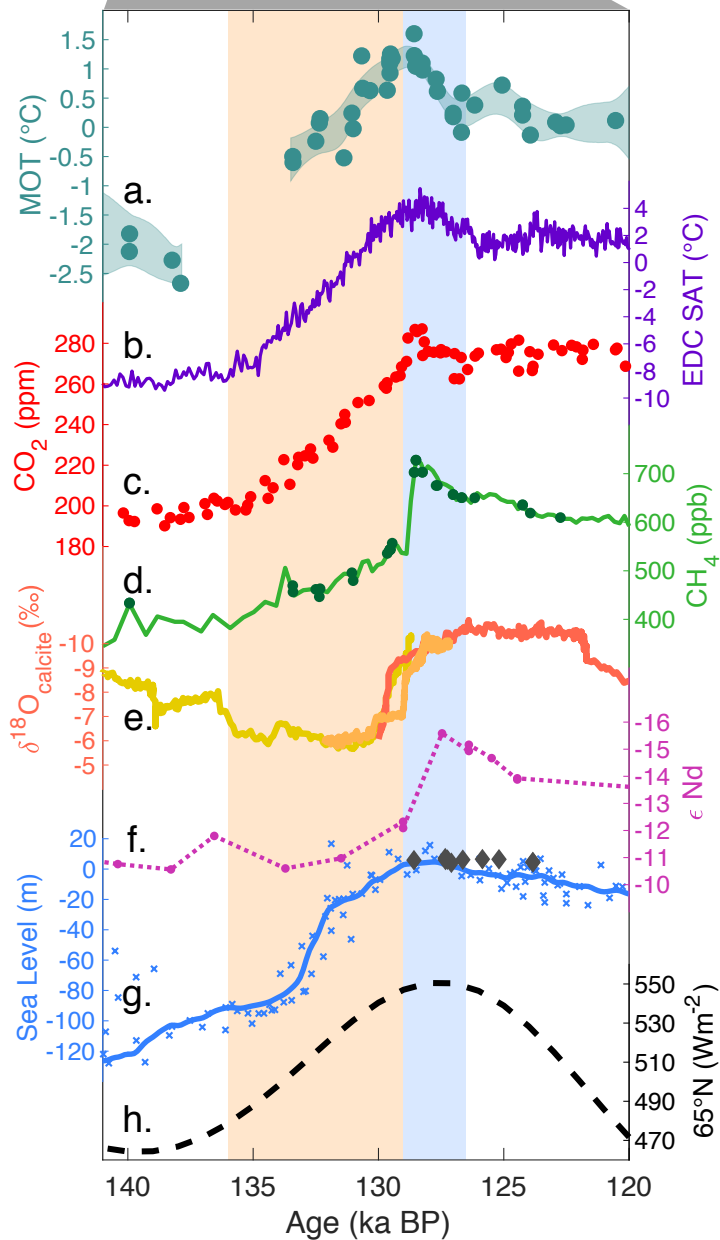
- 627 73. Nilsson, J. *et al.* Ice-shelf damming in the glacial Arctic Ocean : dynamical regimes of a
628 basin-covering kilometre-thick ice shelf. *Cryosph.* **11**, 1745–1765 (2017).
629 74. Kolmogorov, A. N. *Foundations of the Theory of Probability*. (Chelsea Publishing
630 Company, 1950).
631







Termination II



Termination I

